Vorinostat Rescues SQSTM1 Palmitoylation and Restores Dysfunctional Autophagy in Huntington Disease

Yasmeen Alshehabi, Fatima Abrar, Milena Rabu, Anthony Dang, Firyal Ramzan, and Dale D. O. Martin

NeurdyPhagy Lab, Department of Biology, Faculty of Science, University of Waterloo, Waterloo, ON, Canada

Running title: Vorinostat restores autophagy in HD

Correspondance: Dale D. O. Martin, dale.martin@uwaterloo.ca

Keywords: neurodegeneration, autophagy, SQSTM1, p62, Vorinostat, suberoylanilide hydroxamic acid, Huntington disease, palmitoylation, S-acylation

Abstract

Protein mislocalization, dysfunctional autophagy, and protein aggregation are key features of Huntington disease (HD). Accordingly, a central focus of our work has been identifying and correcting the protein mislocalization that drives the underlying autophagic defects which exacerbates protein aggregation. We previously demonstrated that palmitoylation, or S-acylation, of the autophagy receptor sequestosome 1 (SQSTM1; p62) is significantly reduced in the brains of HD patients and the YAC128 HD mouse model, thereby providing a possible mechanism for the cargo-loading failure observed in HD. Here, we identify the FDA-approved small molecule Vorinostat (suberoylanilide hydroxamic acid, SAHA) as a modulator of this pathway and show that it rescues SQSTM1 palmitoylation and restores autophagic function in HD models. Importantly, we demonstrate that Vorinostat crosses the blood-brain-barrier and significantly increases SQSTM1 palmitoylation in the cortices of YAC128 mice using acyl-biotin exchange and click chemistry assays. We further show that Vorinostat enhances autophagic flux, as evidenced by significant changes in autophagy marker levels and a marked increase in the colocalization of huntingtin with SQSTM1 and lysosomes. Finally, we investigate the mechanism of Vorinostat and propose a dual mode of action involving inhibition of depalmitoylating enzymes and transcriptional regulation of key pathway components. Collectively, these findings underscore SQSTM1 palmitoylation as a promising therapeutic target and support Vorinostat as a strong therapeutic candidate in HD.

31 # 1. Introduction

32 Protein aggregation is a hallmark of several neurodegenerative diseases, including Huntington disease
33 (HD), amyotrophic lateral sclerosis (ALS), Alzheimer disease (AD), and Parkinson disease (PD)[1]. While the
34 toxicity of aggregates remains debated, it is well established that the intracellular pathway responsible
35 for their clearance, known as autophagy, is often impaired in these conditions[1–3]. As a result, autophagy
36 has emerged as an attractive therapeutic target for promoting the removal of protein aggregates.
37 However, only stimulating autophagy is insufficient, as it places additional stress on a system that is
38 already compromised. Therefore, effective therapeutic interventions likely require addressing the
39 underlying defects in autophagy while simultaneously increasing autophagic activity. Importantly,
40 mislocalization is increasingly recognized as an early pathogenic event that contributes to proteostasis
41 failure[3–5], making the restoration of protein localization a growing focus for therapeutic development.

42 Macroautophagy, henceforth referred to as autophagy, involves the loading of cargo, such as toxic or
43 aggregated proteins and damaged organelles, into a double-membrane structure known as a
44 phagophore, which seals to form an autophagosome[6] (Figure 1B). This autophagosome is then
45 transported and fused with a lysosome to form the ultimate structure known as an autophagolysosome
46 where the cargo is degraded with hydrolases[6]. The cargo-loading step is crucial, wherein sequestosome
47 1 (SQSTM1; also known as p62) can bind ubiquitinated cargo destined for degradation and deliver it to
48 lipidated microtubule-associated protein 1 light chain 3 (LC3-II) located on the inside of the phagophore
49 membrane[6,7]. In HD, autophagy is dysfunctional at several steps (Figure 1C)[8]. Critically, there is a cargo-
50 loading failure that leads to an accumulation of empty autophagosomes and protein aggregates[9,10].

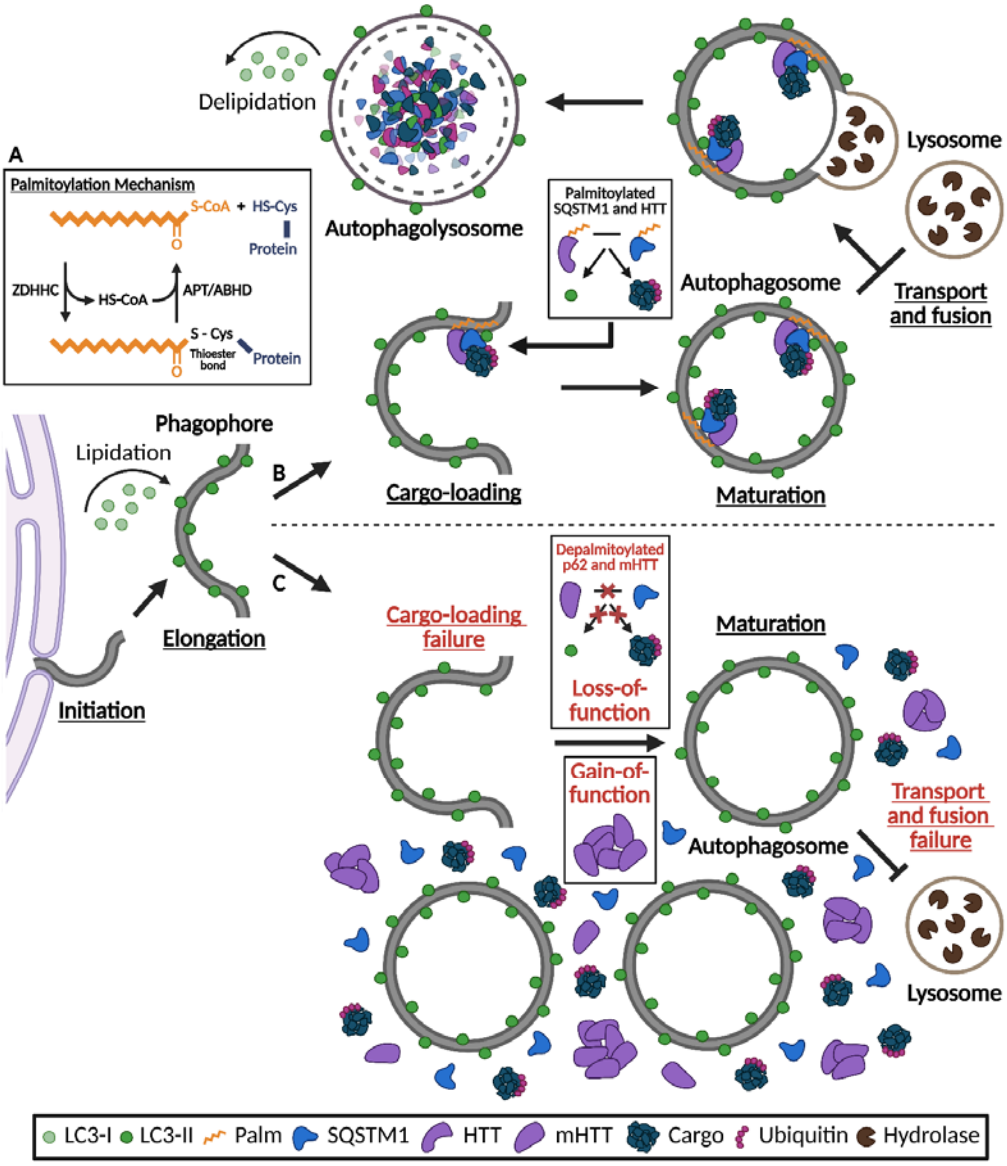

Figure 1 – SQSTM1 and HTT palmitoylation may support healthy autophagy, and its deficiency may contribute to autophagic dysfunction in HD. (A) Palmitoylation involves the formation of a thioester bond between palmitoyl-CoA and a free cysteine residue in a protein via palmitoyl acyltransferases (ZDHHCs). Depalmitoylation involves the cleavage of a thioester bond via acyl protein thioesterases (APTs) or α/β-hydrolase domain enzymes (ABHDs). **(B)** LC3-I undergoes lipidation to form LC3-II, located on both sides of the phagophore membrane. LC3-II then recruits SQSTM1, which can be bound to the ubiquitinated cargo destined for degradation. HTT acts as a scaffold to support the function of SQSTM1. We predict that the palmitoylation of SQSTM1 and HTT plays an important role in their delivery of cargo to the phagophore membrane. Next, the phagophore expands around the cargo and closes to form a sealed autophagosome, which then fuses with a lysosome to form an autophagolysosome. All the contents inside this vesicle are degraded by hydrolytic enzymes, and LC3-II bound to the outside of the double-membrane is released back to the cytosol. **(C)** In HD, there is a defect at the cargo-loading step leading to an accumulation of empty autophagosomes and mHTT aggregates. We predict that this cargo-loading failure is at least partially the result of a reduction in SQSTM1 and HTT palmitoylation. Figure created with Biorender.

67 HD is a neurodegenerative disease with devastating affects on cognition and motor function[11]. HD is an
68 autosomal dominant, monogenic disease caused by a mutation in exon 1 of the huntingtin gene (*HTT*)
69 that encodes a cytosine-adenine-guanine (CAG) repeat expansion (*i.e.,* 36 to 39 CAG repeats for partial
70 HD penetrance; 40 or more repeats for full HD penetrance) resulting in a polyglutamine expansion in the
71 huntingtin protein (HTT)[12,13]. In healthy conditions, HTT is ubiquitous and involved in many cellular
72 processes[14], including autophagy, in which HTT functions as a scaffold, binding to SQSTM1 and
73 ubiquitinated cargo to support the function of SQSTM1 in cargo-loading[2,15–17]. However, cargo-loading is
74 impaired in HD[9,10,17], which may be at least partly due to reduced palmitoylation of SQSTM1 and mHTT[18].
75 We have shown that SQSTM1 palmitoylation plays an important role in cargo-loading and is required for
76 SQSTM1 localization to autophagosomes[7,18,19].

77 Palmitoylation, the most common form of S-acylation, is the reversible post-translational addition of a
78 16-carbon fatty acid to a cysteine residue via a thioester bond[20] (Figure 1A). Due to its reversibility and
79 hydrophobicity, palmitoylation allows selective and dynamic targeting of soluble proteins to membranes
80 and thus plays a key role in regulating protein trafficking[20]. Palmitoylation is mediated by 23 palmitoyl
81 acyltransferases (ZDHHCs) in humans, whereas the reverse reaction is mediated by acyl protein
82 thioesterase (APT), palmitoylprotein thioesterase (PPT), and α/β-hydrolase domain (ABHD) enzymes[21].

83 Notably, SQSTM1 palmitoylation is significantly reduced in the brains of HD patients and YAC128
84 mice[18,19]. In turn, increasing SQSTM1 palmitoylation using broad S-acylation inhibitor Palmostatin B
85 improved HTT and SQSTM1 localization to autophagosomes[18,19]. Moreover, the Hayden group has
86 shown that mHTT palmitoylation is reduced in HD mouse models and further decreases with increasing
87 age and CAG repeat length[22,23]. HTT is palmitoylated by ZDHHC13 and ZDHHC17, and depalmitoylated by
88 APT1 and APT2[22–25]. Importantly, HD is linked to decreased ZDHHC17 activity and increased APT1
89 activity[25,26]. We showed that Palmostatin B restores mHTT palmitoylation and thus mHTT aggregation
90 and cytotoxicity in primary neurons derived from an HD mouse model[23].

91 Like HTT, the Yang group has shown that SQSTM1 is depalmitoylated by APT1[18,27]. In turn, the Saudou
92 group demonstrated that specific inhibition of APT1 using ML348 is protective in the R6/2 HD mouse
93 model overexpressing N-terminal HTT lacking any HTT palmitoylation sites[26]. This suggests that
94 increasing palmitoylation overall is protective. However, targeting palmitoylation in an HD mouse model
95 expressing full length HTT may be more effective due to the relevance of HTT palmitoylation in HD and
96 autophagy. Nevertheless, this study highlights that APT1 may be a therapeutic target in HD independent
97 of HTT. Therefore, the identification of a small molecule which can increase SQSTM1 palmitoylation
98 holds therapeutic promise for HD, rescuing cargo-loading in autophagy, and in turn, reducing mHTT
99 aggregation and toxicity. Through a high-throughput screening of FDA-approved drugs, we identified
100 Vorinostat, also known as suberoylanilide hydroxamic acid (SAHA), as a potential candidate for
101 increasing SQSTM1 palmitoylation[28]. Vorinostat is primarily known as a blood-brain barrier (BBB)
102 permeable inhibitor of lysine deacetylases (KDACs), more commonly known as histone deacetylases
103 (HDACs), which catalyze the removal of acetyl groups (*i.e.,* deacetylation) from lysine residues on
104 proteins, predominantly histones[29,30]. Herein, we report a novel mechanism for Vorinostat, which
105 significantly increases SQSTM1 palmitoylation leading to enhanced autophagic flux. Importantly,
106 Vorinostat crosses the blood-brain barrier and restores SQSTM1 palmitoylation in the brains of YAC128
107 HD mice.

108 ## 2. Materials and Methods

109 ### 2.1 Cell Culture

110 HeLa cells were grown at 37°C in 5% CO_2 in Dulbecco's Modified Eagle Medium (DMEM; Wisent #319-
111 015 CL) supplemented with 10% fetal bovine serum (FBS), 2 mM L-glutamine, 1 mM sodium pyruvate,
112 1X penicillin-streptomycin. Cells were seeded at 170,000 cells per 6 cm plate for biochemistry
113 experiments and 75,000 cells per well onto 0.01 mg/mL poly-D-lysine coated coverslips (#1.5; VWR) in 6-
114 well plates for microscopy experiments. The next day, cells were transfected with 10 µg of plasmid DNA
115 using calcium phosphate precipitation and incubated for 2 hours. The transfection mix contained 1X
116 HEPES-buffered saline (HBS) and 122 mM $CaCl_2$. The media was replaced 2 hours post transfection.
117 Where indicated, drugs were added to transfected cells immediately following the media change and
118 cells were processed 18 hours post transfection (*i.e.,* 16-hour drug incubation). For non-transfected
119 cells, indicated drugs were added for 16 hours prior to processing. Drugs were added at the listed
120 concentrations: 10 µM Vorinostat (Sigma #SML0061), 10 µM ML348 (Cayman #18523), 10 µM
121 Palmostatin B (PalmB; Millipore #178501), 50 µM 2-bromopalmitate (2BP; Sigma #238422), and/or 100
122 nM Bafilomycin A1 (BafA1; Millipore #196000). All drugs were dissolved in dimethyl sulfoxide (DMSO),
123 except for 2BP, which was dissolved in ethanol.

124 ### 2.2 Click Chemistry Assay

125 Cell labeling and click chemistry were performed as previously described[31]. Briefly, 15-hexadecynoic acid
126 (15-HDYA) (Click Chemistry Tools #CCT-1165) was saponified in potassium hydroxide and conjugated to
127 fatty-acid free bovine serum albumin (BSA). Cells were then deprived of lipids in DMEM supplemented
128 with 5% charcoal-stripped FBS (Wisent #080-710), 2 mM L-glutamine, 1 mM sodium pyruvate, 1X
129 penicillin-streptomycin, and incubated with 15-HDYA for 4 hours, after which cells were lysed in
130 modified RIPA buffer (50 mM HEPES pH 7.4, 150 mM NaCl, 2 mM $MgCl_2$, 1% Igepal CA-630, 0.5% sodium
131 deoxycholate, 0.1% SDS). Iodoacetamide was added to each sample to block free cysteine residues.

132 Finally, lysates were subjected to click chemistry with biotin-azide (Click Chemistry Tools #CCT-1488),
133 tris-hydroxypropyl triazolyl methylamine (THPTA; Click Chemistry Tools #CCT-1010), copper sulfate, and
134 sodium ascorbate for 1 hour. The reaction was then ended by acetone precipitation. Since we are
135 looking at total palmitoylated protein, the affinity purification step was skipped, and the protein was
136 denatured at 95°C for 5 minutes in 1X sample loading buffer (SLB) with 20 mM dithiothreitol and stored
137 at -20°C.

138 **2.3 Acyl Biotin Exchange (ABE) Assay**

139 The acyl biotin exchange (ABE) assay was performed as previously described[32]. Briefly, ground cortical
140 brain tissue (approximately 30 mg) was sonicated (3x6 seconds at 20%) in ABE homogenization buffer
141 (10 mM 10X phosphate buffer pH 7.4, 0.32 M sucrose, 1 mM EDTA, 6 M urea, 2.5% SDS) with 1X PIC and
142 20 mM methyl methanthiosulfate (MMTS). Alternatively, cells were sonicated (2x6 seconds at 20%) in
143 lysis buffer (50 mM HEPES pH 7.4, 1 mM EDTA, 2% SDS) with 1X PIC and 20 mM MMTS. Lysates were
144 incubated for 30 minutes at 50°C to block free cysteine residues with MMTS. Excess MMTS was removed
145 by acetone precipitation and resuspended in 4SB (50 mM Tris pH 7.5, 5 mM EDTA, 4% SDS). Samples
146 were then incubated with 0.7 M hydroxylamine and 1 mM HPDP-Biotin (APExBIO #A8008) for 1 hour
147 rotating at room temperature to cleave thioester bonds and label newly freed cysteine residues with
148 biotin. The reaction was ended by acetone precipitation and resuspended in lysis buffer without MMTS.
149 Following protein quantification, 0.5-1 mg of protein was incubated in 150 mM NaCl dilution buffer (50
150 mM HEPES pH 7.0, 1% TX-100, 1 mM EDTA, 1 mM EGTA) with High-Capacity NeutrAvidin Agarose beads
151 (Thermo #29202) for 3 hours rotating at 4°C to bind biotinylated proteins. Following two washes with
152 0.5 M NaCl dilution buffer and one wash with dilution buffer without NaCl, the protein was eluted from
153 beads with elution buffer (dilution buffer, 250 mM NaCl, 0.2% SDS, 1% β-mercaptoethanol) over a 10-
154 minute incubation at 37°C, then denatured at 95°C for 5 minutes in 1X SLB with 1% β-mercaptoethanol
155 and stored at -20°C.

156 **2.4 SDS-PAGE and Western Blotting**

157 12% Bis-Tris polyacrylamide gels were run in 1X XT MOPS buffer (Bio-Rad #1610788) and transferred
158 onto nitrocellulose (to detect SQSTM1) or a polyvinylidene fluoride (to detect LC3-II) membranes via
159 semi-dry transfer using transfer buffer (192 mM glycine, 25 mM tris base, 20% methanol, 0.05% SDS)
160 and the Transblot Turbo Transfer System. Primary antibodies rabbit anti-SQSTM1 (1:1000; Cell Signaling
161 #D1Q5S) or rabbit anti-SQSTM1 (1:1000; Invitrogen #PA5-20839), rabbit anti-LC3A/B (1:1000; Cell
162 Signaling #D3U4C), and mouse anti-VCP (1:1000; Proteintech #60316-1-Ig) were used to detect SQSTM1,
163 LC3-II, and VCP, respectively. Secondary antibodies goat anti-rabbit Starbright 520 (1:2500; Bio-Rad
164 #12005870), donkey anti-rabbit Alexa Fluor 790 (1:2500; Jackson ImmunoResearch #711-655-152), and
165 goat anti-mouse Alexa Fluor 488 (1:2500; Jackson ImmunoResearch #115-545-003) were used. Tubulin-
166 rhodamine (1:5000; Bio-Rad #12004166) was used to detect tubulin as the loading control. Alexa Fluor
167 680 Streptavidin (1:5000; Jackson ImmunoResearch #016-620-084) was used to detect biotinylated
168 proteins.

169 **2.5 Fluorescence Microscopy**

170 For fixed cell imaging, cells were treated with 50 nM LysoTracker Deep Red (Invitrogen #L12492) for 1
171 hour prior to fixation. Cells were washed twice with 1X phosphate buffer saline (PBS), then fixed in 4%
172 paraformaldehyde for 20 minutes at room temperature. Again, cells were washed twice with 1X PBS,
173 then permeabilized in 1X PBS containing 0.1% TX-100, 1 µM $CaCl_2$, 1 µM $MgCl_2$ for 1 minute. Again, cells
174 were washed twice with 1X PBS, then blocked in 0.2% gelatin for 30 minutes. Next, cells were incubated
175 with the primary antibody for 1 hour. Rabbit anti-SQSTM1 (1:500; Invitrogen #PA5-20839) and mouse
176 anti-HTT (1:500; Millipore #MAB2166) were used to detect SQSTM1 and HTT, respectively. Cells were
177 washed twice with 0.2% gelatin, then the last step was repeated with the secondary antibody.
178 Secondary antibodies goat anti-rabbit Alexa Fluor 488 (1:500; Invitrogen) and donkey anti-mouse Alexa
179 Fluor 555 (1:500; Invitrogen) were used. Again, cells were washed twice with 0.2% gelatin, then

180 incubated in 1 µg/mL DAPI (Sigma #D9542) for 20 minutes. Finally, cells were washed twice with 0.2%
181 gelatin. The coverslips were mounted onto microscope slides (Fisher) using ProLong Gold Antifade
182 Mountant (Invitrogen #P36934) and sealed with nail polish. Using a Nikon AXR laser scanning confocal
183 microscope and its NIS-Elements software, Z-stack images were captured at 60X magnification. Next, 3D
184 deconvolution was applied. Protein colocalization was determined by measuring Pearson Correlation
185 Coefficient (PCC) between channels. For HeLa cells, PCC was determined from regions of interest
186 manually drawn around single cells. For neurons, PCC was determined from regions of interest using the
187 automated General Analysis 3 (GA3).

188 **2.6 Molecular Docking**

189 Molecular docking prediction was performed using the AutoDock Vina program[33]. Briefly, the protein
190 PDBQT file was opened in AutoDockTools software to define the grid box dimensions. Molecular docking
191 was then performed using AutoDock Vina via the command prompt, specifying the file path to the
192 program and a folder containing the protein PDBQT file, the ligand PDBQT file, and a text file listing the
193 PDBQT file names, grid box dimension values, energy range, and exhaustiveness. Energy range was set
194 to 4 and exhaustiveness to 64. Running this program produced an "output.pdbqt" file containing the top
195 ligand binding conformations, along with a "log.txt" file listing the corresponding binding affinities.

196 **2.7 qPCR**

197 Total RNA from cells was extracted using RNAZol RT (Bioshop #RNN190). Then, 500 ng of total RNA was
198 used to prepare cDNA using High-Capacity cDNA Reverse Transcription Kit (Applied Biosystems
199 #4368813). Next, cDNA was diluted 1:5, and qPCR was performed using primers and the PowerTrack
200 SYBR Green Master Mix (Applied Biosystems #A46109). Each sample was run in triplicate. qPCR cycling
201 conditions were 2 minutes at 95°C, followed by 40 cycles of 5 seconds at 95°C and 30 seconds at 60°C,
202 then finally 15 seconds at 95°C, 1 minute at 60°C, and 15 seconds at 95°C. The forward and reverse
203 primer sequences were synthesized by IDT and are listed in Table 1. *ACTB* and *GAPDH* were used as

204 housekeeping genes. Primers for the ZDHHCs were previously published[34]. Primers for *SQSTM1*, *HTT*,

205 *VCP*, *MAP1LC3B*, the histone deacetylases, the serine hydrolases, and the housekeeping genes were

206 designed for this study.

207 **Table 1 List of Human Primers for qPCR**

Gene	Forward Sequence (5' to 3')	Reverse Sequence (5' to 3')
ACTB	GCCGCCAGCTCACCA	CTCGTCGCCCACATAGGAAT
GAPDH	TCGGAGTCAACGGATTTGGT	TTCCCGTTCTCAGCCTTGAC
ZDHHC1	CTCACCCGCTCCAGATTGTG	TGAGGCAGGAGGGGAACAAG
ZDHHC2	TGGAGAGAGAGCCAAGAGGAG	TTATAAGTTGGCATCTGTCACAGTATC
ZDHHC3	CTTAACTTCAGTTCGACAGAGTGC	GAAGAGCAGGCCCTCAAAGC
ZDHHC4	GATTGTCTTCATGCTGGGCTTTG	CTCTGTACCACTCGTTAGTAGTCTG
ZDHHC5	GAAGACTGAAGAAAGATAAGAGACATTG	GACACTTCAAAAGTTTACTGTGGATG
ZDHHC6	TCTGCTTGTCCTGGGCTGAG	TGTCTTGGTCTGAAACCCAACC
ZDHHC7	AGTCCATGCTCTGATCCTTTGTG	GGAAGATCAACAGGATTACAGTTATCG
ZDHHC8	TCTGTGACAACTGTGTAGAGGAC	AGCAGGAACAGGAAGAAGTAGC
ZDHHC9	TAGCAATTGGACTTTTGATGATGTTTG	GGGTTTTGCGATTACACGAGAG
ZDHHC11	TCCGTCACCCCAGAAGCCATAC	CGTGAGGCAGGAAGGGAATGAAG
ZDHHC12	TGCTGACCTGGGGAATCACG	CATGAGTGACACAGCGAGGTAG
ZDHHC13	GCATATCTCATCTCAAAGGGACAG	CAACCACATTGAGAGAAGGATTAAAC
ZDHHC14	TCGCTGGCATCCTGTTCTTC	TGCCGTTTGCGATATCTATTTGC
ZDHHC15	TATGAATGAGTCACAGAACCCACTGCTAG	TAATCTTGGTTGTCATCCTCGTTGTCTTCC
ZDHHC16	ATTGTAGCTATCGCCTACCTGTG	AGTAGTGGAAGACAATCAGGATCAG
ZDHHC17	ATGGTTGTGCAACTAATGAAATATGG	GCTATGAGATAAGCAACAATTGAGG
ZDHHC18	CCACCACCGGCCTCTTCTTC	GAGGATGGCAGCGATGATGG
ZDHHC19	GTCCCTGGTTCCTCCCTAGC	AATGCGAAGAAGAGGCCACTG
ZDHHC20	ATCAACCTTTTCCTATCAAACCACTTAG	GCCTTCTTCAGCTCCATTCTCC
ZDHHC21	TCTGGGAATTATGTAACAAGTGTAATTTG	AGAGCCAATGATTATCTTCACCAAC
ZDHHC23	AAAAGTGAACATCAGCATCATCCC	CCAGGAGGAAATGCCAGGAAG
ZDHHC24	CCCCTTCCGAGCTTCTATTGG	CTAGGCCGCTTCCGTATTGG
SQSTM1	GCACTACCGCGATGAGGAC	GCCATCGCAGATCACATTGG
HTT	GCATGGGATCCTGTCCCTTC	GGAGTGTATGGACACCTGGC
VCP	TCTGGAGCCGATTCAAAAGGT	TTCATCCATCTTGGGCTGGG
LYPLA1	CGCTCTTCCTTCCGCTTGC	GCAGGAAAATCACCGCAGC
LYPLA2	AGGCAGCAGAGAACATCAAGG	CAGGTGAGGGCCGTGTAGAG
LYPLAL1	CCTGCATGGCTCAGGTGATT	TCAAGGTGTTCTGGGCAGTC
PPT1	GAAGACCCTGATGGAGGACG	GATCATGGGAGGTGAAGGGC
PPT2	AGACCATCCCAATGCCACAG	CCCGCAGATAAACCAGTTGC
ABHD10	AGCTGATGGGCCACAGATTC	GCATGCTCCACACACCTTTC
ABHD16A	CTCCTGCAGCATCGGTATCC	CGTGTTCTGCCTGGTAGGAG
ABHD17B	TTGCTCTTAGGACAAGATATGGC	ATCAGGAAAGGCAACTCGC

ABHD17C	TTCTACATTGGCCTCGGCTC	GACTCACGCCATACCGGG
HDAC1	TCTATCGCCCTCACAAAGCC	CTCACCAACGTTGAATCTCTGC
HDAC2	GTGAGATTCCCAATGAGTTGCC	GGTGCATGAGGTAACATGCG
HDAC3	ACTACTGTCTGAACGTGCCC	ATTCAACGCATTCCCCATGC
HDAC6	CTATGTCCACCACCAGGCTC	CCCTCATCCAAGGTACAGGC
MAP1LC3B	GCTCATCAAGATAATTAGAAGGCG	GTCTCCTGGGAGGCATAGAC

208 **2.8 Mice**

209 YAC128 transgenic mice on an FVB/N genetic background were obtained from in-house breeding
210 colonies and were originally purchased from the Jackson Laboratory (Strain ID: 004938). Mice were
211 housed in standard laboratory cages under a 12-hour light/dark cycle at 23 ± 1°C, with *ad libitum* access
212 to food and water, and toys for enrichment. All mouse experiments were conducted in accordance with
213 Animal Use Protocol #44651, approved by the UW Animal Care Committee. Mice were administered
214 Vorinostat once every second day between 10 am and 12 pm, at a dose of 50 mg/kg through
215 intraperitoneal (IP) injection (alternating right and left side) for four consecutive weeks for a total of 15
216 treatments[35]. Vorinostat was dissolved in DMSO at a concentration of 40 mg/mL and stored at -20°C. On
217 the day of IP injection, the stock was diluted in corn oil to yield a working solution containing 18.75%
218 DMSO and 81.25% corn oil, with a final Vorinostat concentration of 7.5 µg/µL. Control injections
219 contained the same DMSO-to-corn oil ratio. Solutions were warmed to 37°C for 5 minutes and vortexed
220 for 15 seconds prior to IP injection.

221 **2.9 Mouse-Derived Primary Cortical Neurons**

222 Primary cortical neurons were derived from YAC128 mouse embryos at embryonic day 17. Cortices were
223 dissociated using papain and seeded on 1 mg/mL poly-L-lysine coated wells or glass coverslips (#1.5;
224 Warner) in 6-well plates at 280,000 and 180,000 neurons per well for biochemistry and microscopy
225 experiments, respectively. Neurons were plated in plating media [neurobasal media (Gibco #21103049)
226 supplemented with 2.5% FBS, 2.5% horse serum, 2 mM L-glutamine, 1X penicillin-streptomycin, 2%
227 B27]. The next day, plating media was replaced with neuronal media (neurobasal media supplemented

228 with 2 mM L-glutamine, 1X penicillin-streptomycin, 2% B27). Neurons were processed at 17 days *in*
229 *vitro*.

230 **2.10 Statistics**

231 Statistical analyses and biological repeats are indicated in figure legends. Significant outliers identified
232 using the Grubbs' test were removed and are indicated in figure legends. GraphPad Prism 10 was used
233 for all statistical analyses and graph preparation. Graphs are presented as the standard error of the
234 mean.

235 # 3. Results

236 ## 3.1 Vorinostat increases SQSTM1 palmitoylation but does not affect total protein
237 palmitoylation

238 We identified Vorinostat as a regulator of palmitoylation through a high-throughput screening of FDA-
239 approved drugs. To determine whether Vorinostat regulates autophagic receptor palmitoylation, we
240 examined SQSTM1. Because SQSTM1 is highly dependent on proper localization for its function[6],
241 palmitoylation is a key mechanism regulating protein localization[20], and SQSTM1 palmitoylation is
242 decreased in HD[18,19], we investigated whether Vorinostat could increase SQSTM1 palmitoylation. In turn,
243 an ABE assay was performed to assess SQSTM1 palmitoylation. HeLa cells overexpressing SQSTM1-HA
244 were treated with 10 μM Vorinostat, 10 μM PalmB, or vehicle. PalmB is a broad inhibitor of
245 depalmitoylating enzymes[26], whereas 2BP is a non-specific inhibitor of palmitoylation[36]. The absence of
246 signal in the hydroxylamine (HAM-) lane confirms that without thioester bond cleavage, biotin-HPDP
247 cannot be incorporated on free cysteine residues. Vorinostat treatment led to a significant increase in
248 SQSTM1 palmitoylation (*$p<0.05$) (Figure 2A,B), while PalmB treatment led to no changes.

249 Next, to compare total dynamic palmitoylation in HeLa cells treated with 10 μM Vorinostat, 10 μM
250 ML348, 10 μM PalmB, 50 μM 2BP, or vehicle, we performed click chemistry assays using 15-HDYA.
251 ML348 is a specific inhibitor for APT1[26], the enzyme that depalmitoylates SQSTM1[18,27]. The absence of a
252 signal in the cold palmitate (palm) lane confirms that without an alkyne group, biotin-azide cannot be
253 added to the palmitate. Vorinostat treatment led to no changes in total protein palmitoylation (Figure
254 2C,D). ML348 and 2BP treatments led to a slight decrease in total protein palmitoylation, whereas
255 PalmB led to a slight increase. Overall, these finding suggest that Vorinostat may promote
256 palmitoylation of a subset of proteins, including SQSTM1.

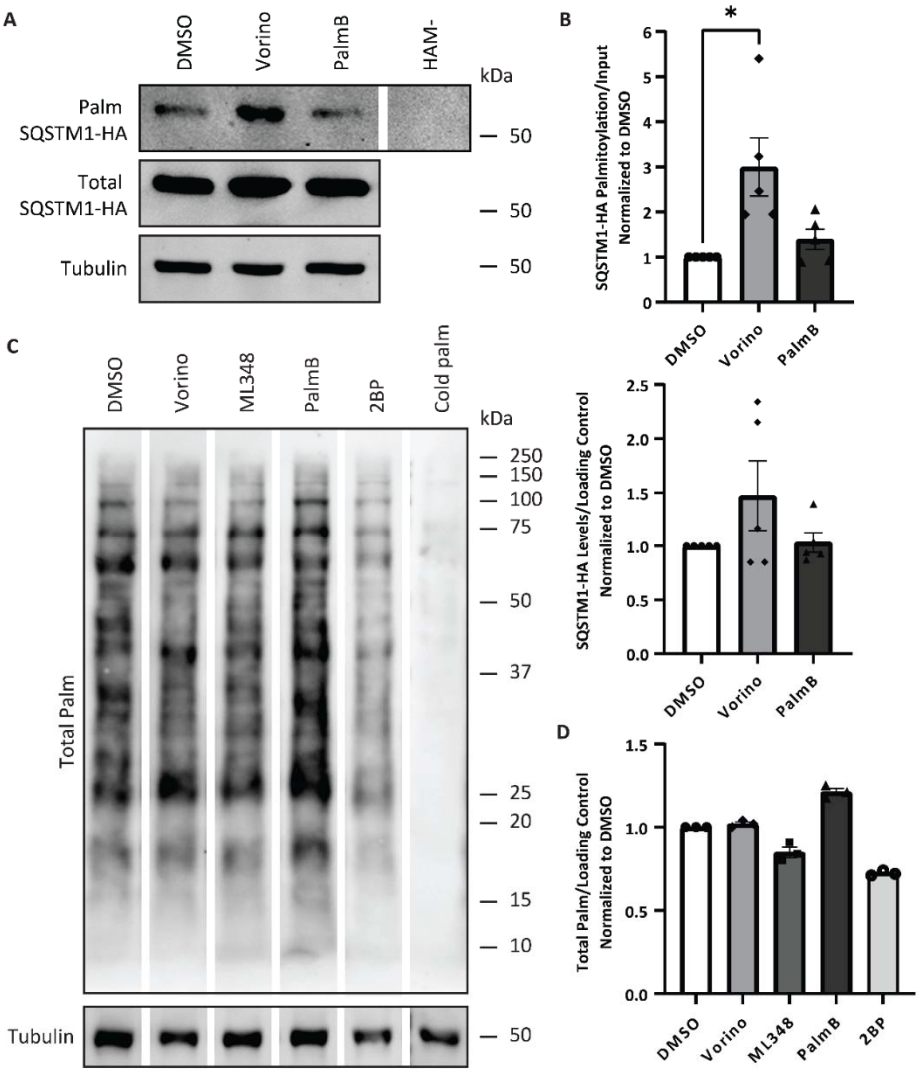

Figure 2 – Vorinostat increases SQSTM1 palmitoylation but does not affect total protein palmitoylation. (A) SQSTM1 palmitoylation was detected via acyl biotin exchange assay using HeLa cells overexpressing SQSTM1-HA and treated with 10 µM Vorinostat, 10 µM PalmB, or vehicle. Composite of the same gel. **(B)** Quantification of (top) SQSTM1 palmitoylation and (bottom) SQSTM1 levels from five biological replicates. Kruskal-Wallis test followed by Dunn's post-hoc analysis. **(C)** Total palmitoylated protein was detected via click chemistry using HeLa cells treated with 10 µM Vorinostat, 10 µM ML348, 10 µM PalmB, 50 µM 2BP, or vehicle in presence of 15-HDYA. Composite of the same gel. **(D)** Quantification of total palmitoylated protein from three biological replicates. Kruskal-Wallis test followed by Dunn's post-hoc analysis.

267 **3.2 Vorinostat crosses the blood-brain barrier and increases SQSTM1 palmitoylation in**
268 **YAC128 HD mice**

269 *In vitro*, Vorinostat increased SQSTM1 palmitoylation (Section 3.1). We next sought to determine
270 whether Vorinostat crosses the blood-brain barrier and exerts the same effect *in vivo* in the YAC128 HD
271 mouse model. We also examined valosin-containing protein (VCP). VCP has been identified in palmitoyl-
272 proteomic studies[37,38] and plays important roles in autophagy[39]. Moreover, VCP is the major pathogenic
273 protein in multisystem proteinopathy (MSP)[40] and one of the several pathogenic proteins implicated in
274 amyotrophic lateral sclerosis (ALS)[41]. Therefore, we investigated whether Vorinostat also increases VCP
275 palmitoylation in addition to SQSTM1. 22-month-old YAC128 mice were administered 50 mg/kg
276 Vorinostat or vehicle via intraperitoneal injection once every second day for four consecutive weeks.
277 Subsequently, an ABE assay was performed using the mouse cortices. Vorinostat treatment in YAC128
278 mice led to a significant increase in SQSTM1 and VCP palmitoylation (*$p<0.05$) compared to YAC128
279 vehicle-treated and WT Vorinostat-treated mice (Figure 3A,B). Vorinostat treatment in WT mice did not
280 affect SQSTM1 and VCP palmitoylation, nor total protein palmitoylation in both WT and YAC128 mice.

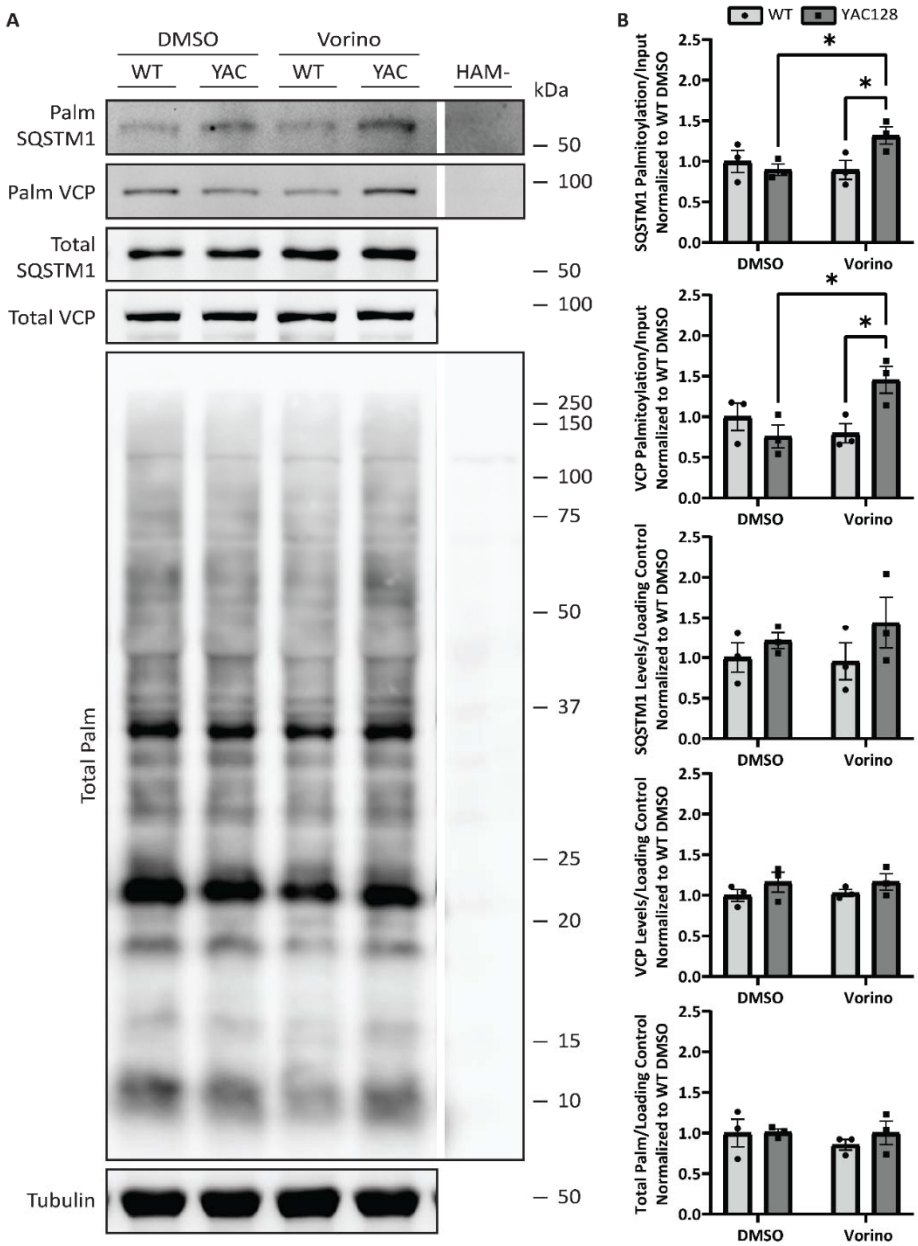

Figure 3 – Vorinostat crosses the blood-brain barrier and increases SQSTM1 palmitoylation in YAC128 mice. (A) SQSTM1 palmitoylation was detected via acyl biotin exchange assay using cortices from YAC128 mice that were administered 50 mg/kg Vorinostat or vehicle every other day for 4 consecutive weeks. Composite of the same gel. **(B)** Quantification of (top) SQSTM1 palmitoylation, (second) VCP palmitoylation, (third) SQSTM1 levels, (fourth) VCP levels, and (bottom) total palmitoylated protein from three biological replicates. Two-way ANOVA test followed by Fisher's LSD post-hoc analysis (*$p<0.05$).

3.3 Vorinostat induces autophagy and redirects HTT to lysosomes

Given that Vorinostat increases SQSTM1 palmitoylation in YAC128 mice, we next examined its effect on autophagy. In autophagy, SQSTM1 is degraded in autophagolysosomes, and while some of LC3-II located

291 on the inner surface is also degraded, the majority located on the outer surface is recycled back to LC3-I,
292 the inactive delipidated form of LC3[42]. This makes SQSTM1 and LC3-II excellent markers of autophagy,
293 such that increased autophagic flux is indicated by reduced SQSTM1 levels and elevated LC3-II levels[42].
294 BafA1 is a late-stage autophagy inhibitor that prevents autophagosome-lysosome fusion leading to an
295 increase in both SQSTM1 and LC3-II levels[42]. BafA1 is used to confirm that the effect of the drug
296 treatment on autophagic flux is indeed a result of increased autophagy[42]. HeLa cells were treated with
297 10 µM Vorinostat, 10 µM ML348, 10 µM PalmB, or vehicle, with or without BafA1. Vorinostat treatment
298 led to a significant decrease in SQSTM1 levels (*$p<0.05$) (Figure 4A,B), with a concomitant significant
299 increase in LC3-II levels (*$p<0.05$), indicating autophagy has been induced and SQSTM1 is being
300 degraded in the autophagolysosome. ML348 and PalmB treatment led to no changes in SQSTM1 or LC3-
301 II levels. All BafA1 treatment conditions led to a significant increase in LC3-II (**$p<0.01$) and SQSTM1
302 (***$p<0.001$).

303 Furthermore, an indicator of functional autophagy is the colocalization of SQSTM1, HTT, and lysosomes,
304 which suggests that SQSTM1 is successfully delivering cargo (*e.g.,* mHTT) with the support of HTT to
305 autophagosomes, which fuse with lysosomes to form autophagolysosomes. Therefore, increased
306 colocalization between these proteins and organelles, as measured by the PCC, indicates enhanced
307 autophagic flux, as the presence of SQSTM1 and HTT in lysosomes signifies their successful delivery.
308 Consequently, HeLa cells were treated with 10 µM Vorinostat, 10 µM ML348, 10 µM PalmB, or vehicle
309 and visualized by fixed cell confocal immunofluorescence microscopy. When treated with Vorinostat,
310 ML348, or PalmB, SQSTM1 and HTT colocalization significantly increased, with a more pronounced
311 increase elicited by Vorinostat (****$p<0.0001$) (Figure 4C,D). When treated with Vorinostat or PalmB,
312 SQSTM1 and lysosome colocalization significantly increased, with a more pronounced increase detected
313 in Vorinostat treated cells (****$p<0.0001$). ML348 had no effect on SQSTM1 and lysosome

314 colocalization. Finally, when treated with Vorinostat, ML348, or PalmB, HTT and lysosome colocalization
315 significantly increased, with a greater increase induced by Vorinostat (****p<0.0001).

316 To confirm the effect in HD, primary cortical neurons derived from WT and YAC128 mice were treated
317 with 10 µM Vorinostat, 10 µM ML348, 10 µM PalmB, or vehicle and visualized by fixed cell confocal
318 immunofluorescence microscopy. In WT cortical neurons treated with Vorinostat, SQSTM1 and HTT
319 colocalization was not affected (Figure 5A,C). However, in YAC128 cortical neurons treated with
320 Vorinostat, SQSTM1 and HTT colocalization significantly increased (***p<0.001). Similarly, SQSTM1 and
321 lysosome colocalization was not affected with Vorinostat treatment in WT cortical neurons but
322 significantly increased (**p<0.01) in YAC128 cortical neurons. In addition, HTT and lysosome
323 colocalization, which includes both HTT and mHTT in YAC128 cortical neurons, was not affected with
324 Vorinostat treatment in WT cortical neurons but significantly increased (****p<0.0001) in YAC128
325 cortical neurons, which is especially relevant in this context where colocalization suggests that mHTT will
326 be degraded in autophagolysosomes. When treated with ML348, WT cortical neurons showed
327 significantly increased SQSTM1 and HTT colocalization (**p<0.01), but not HTT and lysosome or SQSTM1
328 and lysosome colocalization. Whereas YAC128 cortical neurons showed significantly increased SQSTM1
329 and HTT colocalization (***p<0.001), as well as HTT and lysosome colocalization (**p<0.01), but not
330 SQSTM1 and lysosome colocalization. When treated with PalmB, WT cortical neurons had significantly
331 increased SQSTM1 and HTT colocalization (**p<0.01), as well as HTT and lysosome colocalization and
332 ****p<0.0001), but not SQSTM1 and lysosome colocalization. Whereas YAC128 cortical neurons showed
333 significantly increased HTT and lysosome colocalization (***p<0.001), but not SQSTM1 and HTT or
334 SQSTM1 and lysosome colocalization. Overall, these results suggest that increasing total palmitoylation
335 in YAC128 cortical neurons directs HTT to SQSTM1 and lysosomes; however, only Vorinostat was
336 effective at redirecting both SQSTM1 and HTT together and to lysosomes, and to a much greater extent.

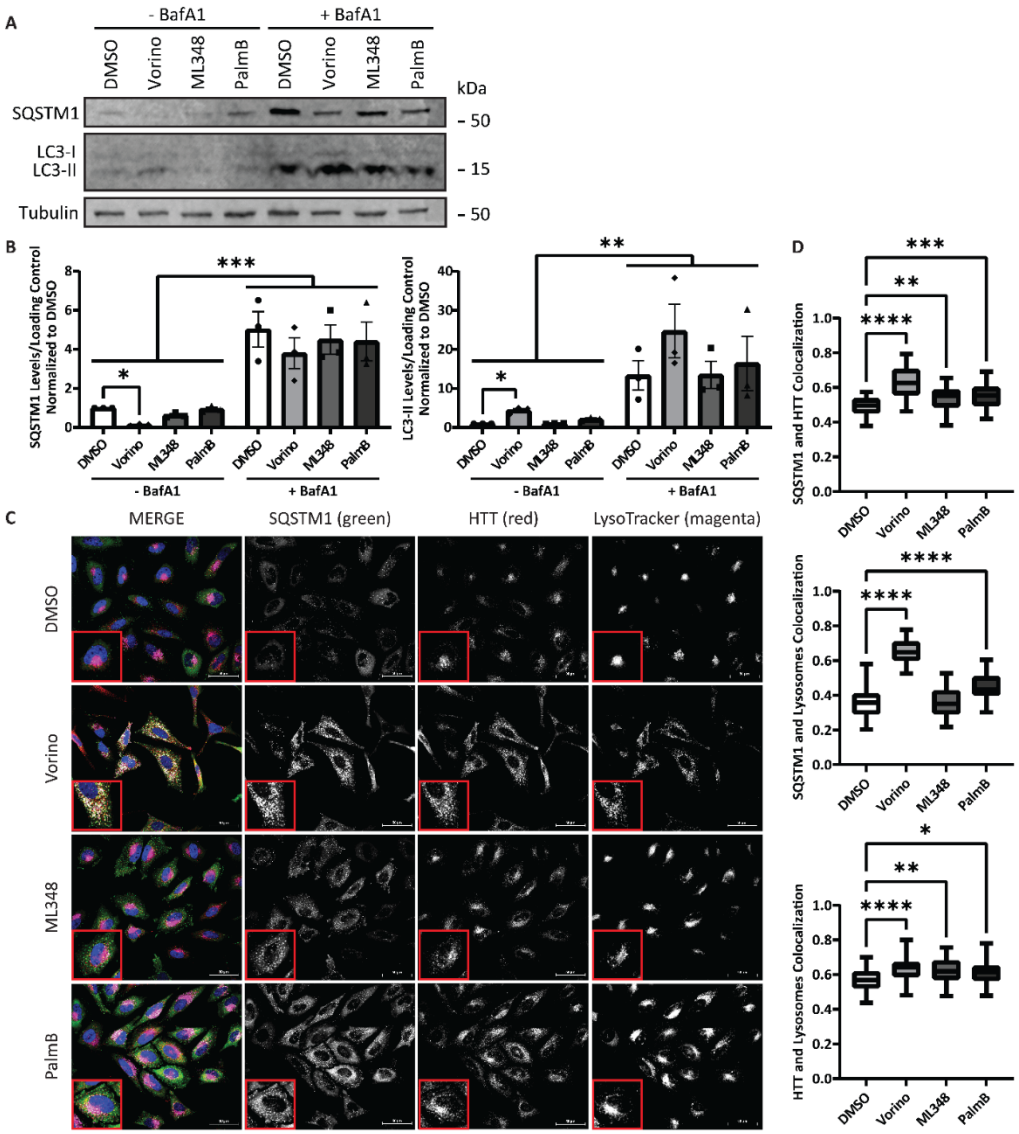

Figure 4 – Vorinostat increases autophagic flux. (A) SQSTM1 and LC3-II levels were detected in HeLa cells treated with 10 µM Vorinostat, 10 µM ML348, 10 µM PalmB, or vehicle, with or without BafA1. **(B)** Quantification of (left) SQSTM1 levels and (right) LC3-II levels from three biological replicates. Kruskal-Wallis test followed by Dunn's post-hoc analysis (*p<0.05) within +/- BafA1 conditions. Two-way ANOVA test followed by Fisher's LSD post-hoc analysis (**p<0.01, ***p<0.001) across BafA1 conditions. **(C)** SQSTM1, HTT, and lysosomes were visualized via confocal immunofluorescence microscopy using fixed HeLa cells treated with 10 µM Vorinostat, 10 µM ML348, 10 µM PalmB, or vehicle. **(D)** Quantification of (left) PCC between SQSTM1 and HTT, (middle) PCC between SQSTM1 and lysosome, and (right) PCC between HTT and lysosome, 15 cells per condition from three biological replicates. One-way ANOVA test followed by Dunnett's post-hoc analysis (*p<0.05, **p<0.01, ***p<0.001, ****p<0.0001). Box and whiskers (min to max).

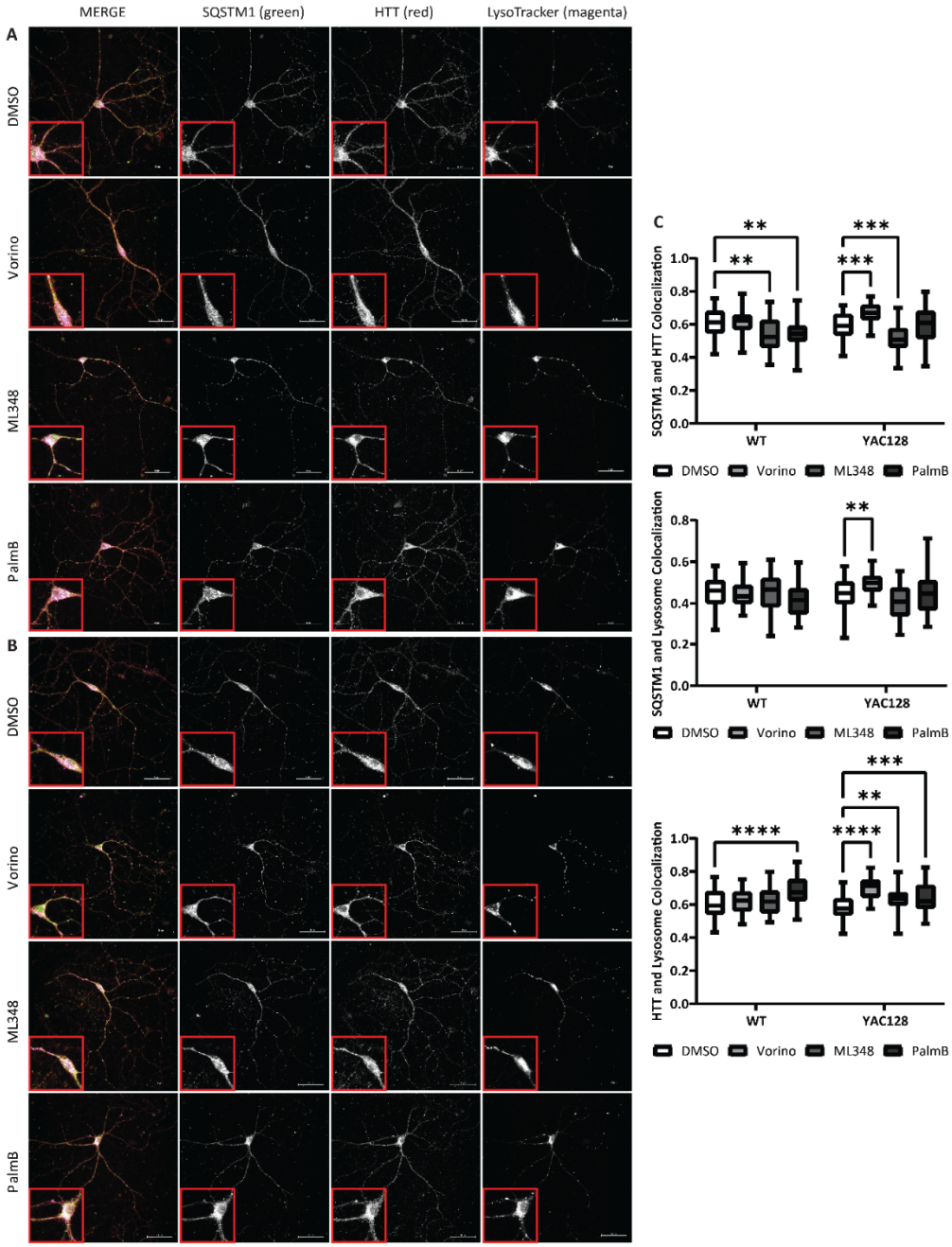

Figure 5 – Vorinostat redirects HTT and SQSTM1 to lysosomes in HD neurons. SQSTM1, HTT, and lysosomes were visualized via confocal immunofluorescence microscopy using fixed primary cortical neurons derived from **(A)** WT and **(B)** YAC128 mouse embryos treated with 10 µM Vorinostat, 10 µM ML348, 10 µM PalmB, or vehicle. **(C)** Quantification of (top) PCC between SQSTM1 and HTT, (middle) PCC between SQSTM1 and lysosome, and (bottom) PCC between HTT and lysosome, on an average of 15 neurons per condition from three biological replicates. Two-way ANOVA test followed by Dunnett's post-hoc analysis (**p<0.01, ***p<0.001, ****p<0.0001). Box and whiskers (min to max).

357 **3.4 Vorinostat may function as a depalmitoylation inhibitor and transcriptional regulator**

358 SQSTM1 has been shown to be depalmitoylated by APT1[18,27]. Thus, our initial theory was Vorinostat may
359 function via inhibition of APT1, thereby increasing SQSTM1 palmitoylation. To further investigate,
360 molecular docking experiments were performed using AutoDock Vina. These results indicate that
361 ML348, an inhibitor specific to APT1[26], and Vorinostat have a deep fit into the binding pocket of APT1,
362 with ML348 exhibiting a stronger binding affinity (-10.6 kcal/mol) compared to Vorinostat (-8.0 kcal/mol)
363 (Figure 6A). We also looked at APT2 for comparison and found that ML349, an inhibitor specific to
364 APT2[26], and Vorinostat have a deep fit into the binding pocket of APT2, with ML349 exhibiting a stronger
365 binding affinity (-12.9 kcal/mol) compared to Vorinostat (-8.0 kcal/mol). For context, the more negative
366 the value, the stronger the binding affinity.

367 Alternatively, Vorinostat is already known as an HDAC inhibitor[29,30], so its function could be through
368 increasing the transcription of palmitoylating enzymes or decreasing the transcription of
369 depalmitoylating enzymes. To further investigate, qPCR was performed using HeLa cells treated with 10
370 µM Vorinostat or vehicle to quantify the relative transcript levels of *ZDHHC1-24*, *SQSTM1*, *HTT*, *VCP*,
371 *LYPLA1* (APT1), *LYPLA2* (APT2), *PPTs*, *ABHD*s, *HDAC*s, and *MAP1LC3*s (Figure 6B,C). Compared to vehicle,
372 treatment with Vorinostat led to significantly increased *ZDHHC11*, *ZDHHC23*, and *SQSTM1* transcript
373 levels, as well as significantly decreased transcript levels of *ZDHHC2*, *ZDHHC4*, *ZDHHC5*, *ZDHHC9*,
374 *ZDHHC16*, *ZDHHC17*, *ZDHHC18*, *ZDHHC20*, *ZDHHC21*, *VCP*, *LYPLA2*, *PPT1, PPT2*, *ABHD16A,* and *ABHD17C*.
375 Notably, *HTT*, *LYPLA1*, and *ZDHHC19* transcript levels were unaffected by Vorinostat treatment.
376 ZDHHC22 had amplification in the Vorinostat condition, but not vehicle condition, whereas ABHD17A
377 and MAP1LC3A showed no amplification in either condition.

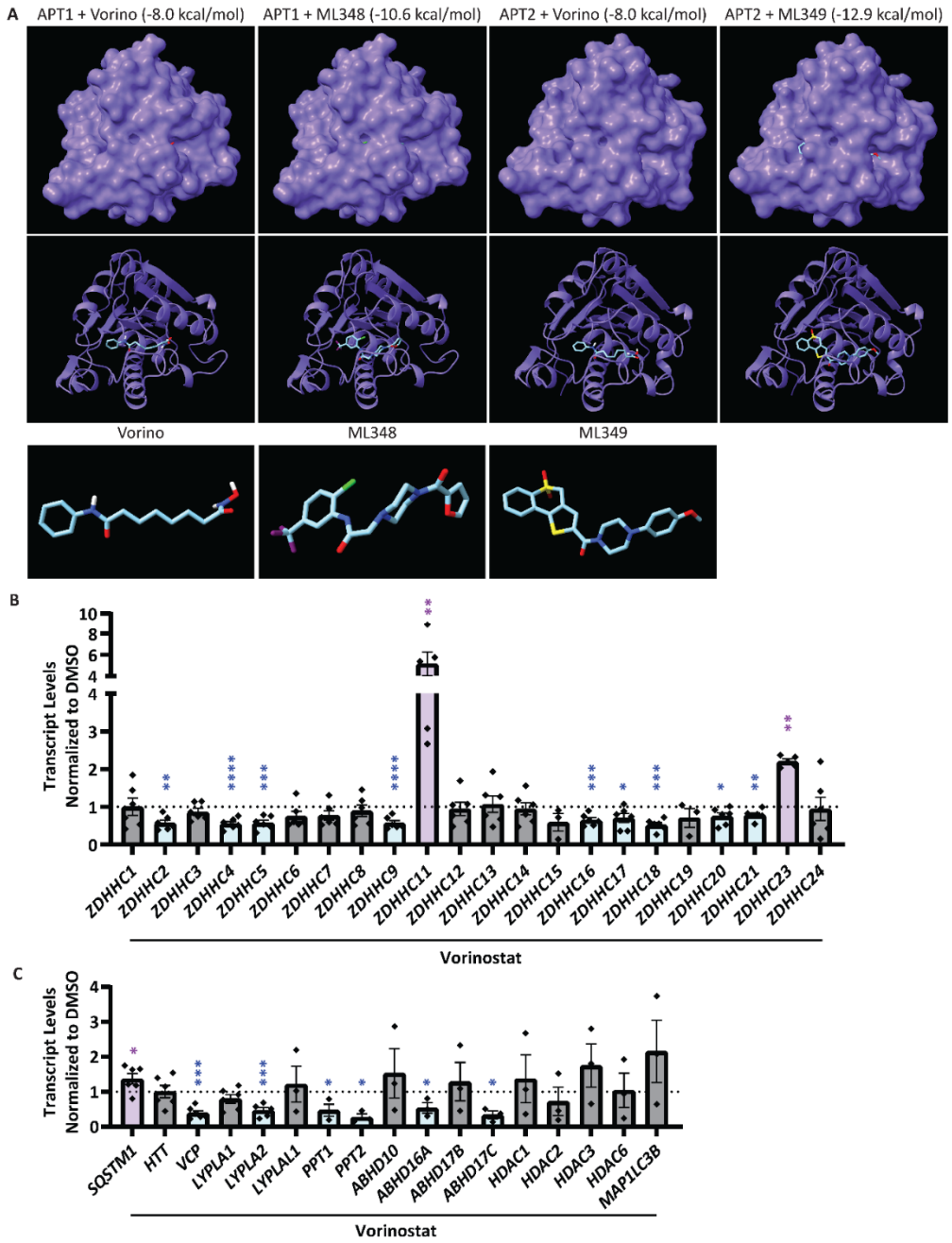

Figure 6 – Vorinostat may function as a depalmitoylation inhibitor and transcriptional regulator. (A) Vorinostat and ML348 molecular docking and binding affinity on APT1 and APT2 were predicted using AutoDock Vina. **(B)** *ZDHHC1-24* transcript levels were detected via qPCR using HeLa cells treated with 10 µM Vorinostat or vehicle. *ZDHHC2,4,5,9,11,16,17,18,20,21,23* transcript levels are sensitive to Vorinostat treatment. One significant outlier (SO) removed from ZDHHC11 and ZDHHC23. Two-tailed unpaired *t*-test (*p<0.05, **p<0.01, ***p<0.001, ****p<0.0001). **(C)** *SQSTM1*; *HTT; VCP*; *LYPLA1,2*; *LYPLAL1*; *PPT1,2*; *ABHD10,16A,17A,17B,17C*; *HDAC1,2,3,6*; and *MAP1LC3A,B* transcript levels were detected via qPCR using HeLa cells treated with 10 µM Vorinostat or vehicle. *SQSTM1*, *VCP*, *LYPLA2*, *PPT1*, *PPT2*, *ABHD16A*, and *ABHD17C* transcript levels are sensitive to Vorinostat treatment. One SO removed from LYPLA2. Two-tailed unpaired *t*-test (*p<0.05, ***p<0.001).

389 ## 4. Discussion

390 Autophagy is disrupted in HD at various stages[8]. In particular, a failure at the cargo-loading step has
391 been linked to SQSTM1's inability to deliver cargo to the phagophore membrane for degradation
392 resulting in an accumulation of empty autophagosomes[9,10]. Since palmitoylation plays an important role
393 in protein localization to membranes[20], we predicted that the autophagic dysfunction seen in HD is
394 linked to reduced SQSTM1 palmitoylation detected in the brains of HD patients and YAC128 mice[18,43].
395 Consequently, we sought to promote mHTT intracellular degradation, thereby preventing cytotoxicity
396 and neuronal death, by restoring SQSTM1 palmitoylation. Through a high-throughput screening of FDA-
397 approved drugs, we identified blood-brain permeable Vorinostat as a candidate to increase SQSTM1
398 palmitoylation.

399 We found that Vorinostat treatment significantly increases SQSTM1 palmitoylation but does not affect
400 total protein palmitoylation both *in vitro* (Figure 2) and *in vivo* (Figure 3). Since the biochemical assays
401 for our *in vivo* work were conducted on cortical tissue, this confirms that Vorinostat successfully crosses
402 the blood-brain barrier. Notably, PalmB did not increase SQSTM1 palmitoylation *in vitro*. This may be
403 because PalmB is a broad inhibitor of depalmitoylating enzymes[26]. Since many palmitoylating enzymes
404 undergo regulatory palmitoylation (*e.g.,* ZDHHC6 is palmitoylated by ZDHHC16[44] and ZDHHC5 is
405 palmitoylated by ZDHHC20[45]), broad inhibition of depalmitoylating enzymes could disrupt the function
406 of palmitoylating enzymes, potentially explaining the lack of effect of PalmB on SQSTM1 palmitoylation.

407 With an increase in SQSTM1 palmitoylation induced by Vorinostat treatment, we then observed a
408 corresponding increase of autophagic flux. We found that Vorinostat treatment significantly decreases
409 SQSTM1 levels and increases LC3-II levels (Figure 4). SQSTM1 and LC3-II are autophagy markers, and
410 their respective decrease and increase in levels suggests increased autophagic flux, since SQSTM1 is
411 degraded in autophagolysosomes, whereas the majority of LC3-II is recycled back into the inactive

412 delipidated form of LC3[42]. Increased autophagic flux was confirmed with Vorinostat plus BafA1
413 treatment, a late-stage autophagy inhibitor[42], which significantly increased SQSTM1 and LC3-II levels.

414 Furthermore, with an increase in SQSTM1 palmitoylation induced by Vorinostat treatment, we then
415 observed a corresponding enhancement of autophagy. We found that Vorinostat treatment significantly
416 increased SQSTM1, HTT, and lysosome colocalization in HeLa cells (Figure 4), as well as primary cortical
417 neurons derived from YAC128 mice, but not WT mice (Figure 5). In HeLa cells, this suggests enhanced
418 SQSTM1 and HTT delivery to autophagosomes. In YAC128 primary cortical neurons, increased SQSTM1,
419 HTT, and lysosome colocalization suggests improved delivery of HTT to autophagosomes for subsequent
420 degradation in autophagolysosomes. Notably, the observation that Vorinostat had an effect in YAC128
421 but not in WT primary cortical neurons is important as it suggests that Vorinostat may exert its effects
422 selectively under pathological conditions, reducing the risk of potential off-target effects. The effects of
423 ML348 and PalmB on SQSTM1, HTT, and lysosome colocalization were neither as strong, consistent, nor
424 specific as those of Vorinostat, suggesting that Vorinostat may be a more effective drug in HD.

425 Initially, we predicted that Vorinostat increases SQSTM1 palmitoylation by acting as a depalmitoylation
426 inhibitor, specifically of APT1, the depalmitoylating enzyme of SQSTM1. Consequently, we aimed to
427 better understand Vorinostat's ability to inhibit depalmitoylating enzymes through molecular docking
428 experiments to quantify Vorinostat's binding affinity to APT1 and APT2 (Figure 6). Although Vorinostat
429 had a deep fit into the binding pockets of both APT1 and APT2, its binding affinity to either was weaker
430 than that of the specific inhibitors, ML348 and ML349. However, prior experiments indicated that
431 Vorinostat was more effective than ML348 at increasing SQSTM1 palmitoylation, thus prompting us to
432 reassess our previous thinking. Vorinostat is also a known HDAC inhibitor, promoting histone acetylation
433 or transcription factor acetylation, thereby increasing transcription[29,30]. Either way, Vorinostat could
434 increase the transcription of *ZDHHC* genes, leading to increased SQSTM1 palmitoylation through an
435 alternative pathway. Hence, Vorinostat may be acting via a dual mechanism, as summarized in Figure 7.

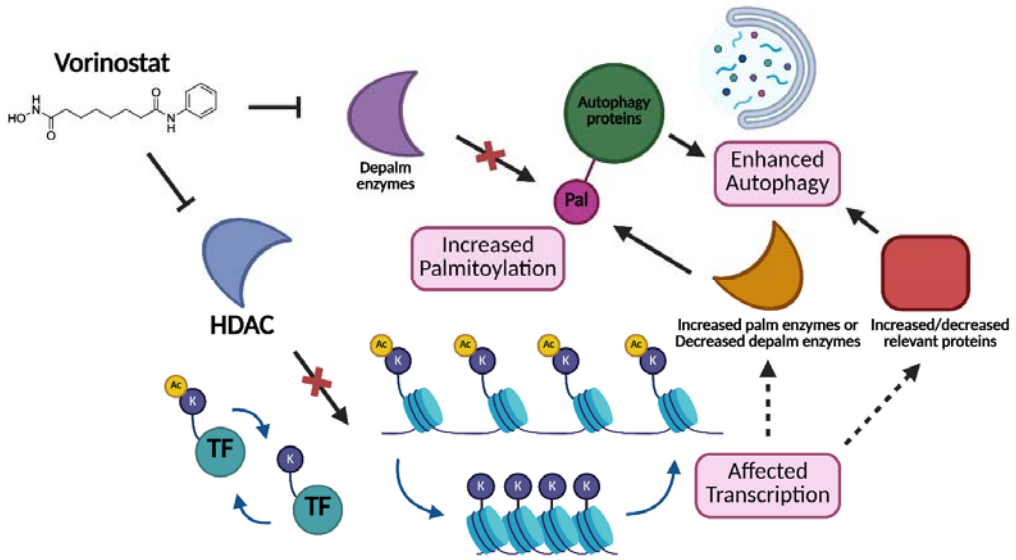

Figure 7 – Predicted Vorinostat mechanism. Vorinostat may be working through two concurrent mechanisms to increase autophagy protein palmitoylation: inhibition of depalmitoylating (depalm) enzymes and inhibition of acetylation enzymes (HDAC). Inhibition of depalmitoylating enzymes prevents the depalmitoylation of SQSTM1, thus increasing SQSTM1 palmitoylation. In contrast, inhibition of HDAC prevents deacetylation of histones, thereby increasing their acetylation, promoting active transcription by opening chromatin. Alternatively, inhibition of HDAC prevents deacetylation of transcription factors (TF), thus increasing their acetylation, also promoting active transcription (K represents a lysine residue protruding from the histone, and Ac represents an acetyl group). This may increase transcription of palmitoylating (palm) enzymes or decrease the transcription of depalmitoylating enzymes, overall increasing autophagy protein palmitoylation. Alternatively, this may increase or decrease transcription of relevant proteins, such as SQSTM1, which may also enhance autophagy. Figure generated on BioRender.

The next step was to confirm whether Vorinostat increases transcription of relevant proteins by quantifying transcript levels via qPCR. We found that Vorinostat significantly increases *SQSTM1* transcript levels compared to vehicle, suggesting that Vorinostat may promote autophagy. However, Vorinostat plus BafA1 did not lead to an increase in SQSTM1 levels (Figure 4). It could be that Vorinostat plus BafA1 leads to the accumulation of detergent-insoluble SQSTM1, as described by the Yang group[27], which may limit detection of SQSTM1 via western blot. In addition, we found that Vorinostat significantly increases *ZDHHC11* and *ZDHHC23* transcript levels compared to vehicle. Work by the Liu group suggests that ATG2A is palmitoylated by ZDHHC11 and its *depalmitoylation* is required for proper autophagosome formation[46]. In contrast, studies by the Kim group suggest that MCOLN3/TRPML3 is

458 palmitoylated by ZDHHC11 and its *palmitoylation* is required for proper autophagosome formation[47].
459 Minimal connections between ZDHHC23 and autophagy have been established. Therefore, it remains
460 unclear how Vorinostat-induced increases in the *ZDHHC11* and *ZDHHC23* transcript levels might have a
461 role in the increase and enhanced autophagy we observed following Vorinostat treatment. Furthermore,
462 we found that Vorinostat decreases *LYPLA2* transcript levels which encode APT2. APT2 depalmitoylates
463 HTT, and HTT palmitoylation is reduced in HD mouse models[23]. Therefore, reducing APT2 may increase
464 HTT palmitoylation, thereby lowering mHTT aggregation and cytotoxicity. Although increased transcript
465 levels do not necessarily equate to increased protein levels, they serve as a good representation of
466 potential regulatory changes at the transcriptional level and can provide insight into upstream effects of
467 Vorinostat treatment.

468 **4.1 Vorinostat and Huntington disease**

469 Vorinostat has been tested in HD mouse models previously, but in the context of its HDAC inhibiting
470 properties and fixing transcriptional dysregulation found in HD[35,48]. The Bates group treated the R6/2 HD
471 mouse model with Vorinostat and found it restored motor impairment, reduced mHTT aggregates in the
472 cortex, and restored *Bdnf* transcript levels[35,48]. Similarly, the Saudou group found restored BDNF
473 trafficking with APT1 inhibition by ML348 in the R6/2 model[26]. BDNF is implicated in HD pathogenesis[49].
474 In R6/2 mice, *Bdnf* transcript levels decline during disease progression[50]; accordingly, BDNF over-
475 expression was found to improve HD phenotypes[51]. The Bates group also found that Vorinostat
476 decreases HDAC2 and HDAC4 levels *in vivo*[48]. In R6/2 mice, the group reported that HDAC4 associates
477 with mHTT in a polyQ-dependent manner and colocalizes with cytoplasmic inclusions, and knockdown of
478 HDAC4 reduced cytoplasmic aggregate formation, restored *Bdnf* transcript levels, rescued membrane
479 properties of MSNs and of corticostriatal synaptic transmission, improved motor and neurological
480 impairment, and extended the lifespan of R6/2 mice[52]. Of note, the R6/2 model only expresses the very
481 N-terminus of HTT, which does not include any palmitoylation sites[24] or SQSTM1 binding sites[17].

482 To further understand the mechanism of HDAC4, the Cristea group studied its interaction in the context
483 of HD through multiomics and proposed a potential model of the role for HDAC4 in HD[53]. One notable
484 finding from their study is the interaction between HDAC4 and VCP, which they also found has minimal
485 interaction in the Q20 WT mice and maximal interaction in the Q140 HD mice, an interaction which
486 increases with age. Combining this with our findings on VCP, it is possible that the increased interaction
487 between HDAC and VCP, and likely VCP acetylation[54], interferes with VCP palmitoylation, thereby
488 disrupting its normal function. By deceasing HDAC4 levels with Vorinostat, VCP function may be
489 restored.

490 **4.2 VCP and Huntington disease**

491 VCP is involved in autophagy initiation[39] and HD[55]. The Qi group identified VCP as a mHTT-binding
492 protein on mitochondria, where it drives excessing mitophagy, or the autophagic degradation of
493 mitochondria[55]. Because palmitoylation is a key regulator of protein localization[20], restoring VCP
494 palmitoylation could potentially correct its mislocalization, reducing VCP accumulation on mitochondria
495 in HD mouse models. Thus, we looked at whether Vorinostat also rescues VCP palmitoylation in addition
496 to SQSTM1 palmitoylation and found that, *in vivo*, Vorinostat treatment significantly increases VCP
497 palmitoylation.

498 **4.3 Future Directions**

499 Although studies have demonstrated positive outcomes of Vorinostat treatment in HD mouse models,
500 the broader consequences of HDAC inhibition remain an important consideration. Determining the
501 specific mechanism by which Vorinostat mediates these positive effects should be a priority, as this
502 knowledge could guide the design of more targeted small molecules. However, it is also possible that
503 Vorinostat's multi-functional nature contributes to its broad impact on various HD phenotypes, whether
504 through restoring protein palmitoylation, correcting transcriptional dysregulation, or both. In this study,

505 we reported that Vorinostat crossed the blood-brain barrier and increased SQSTM1 palmitoylation *in*
506 *vivo*, as well as enhanced autophagy *in vitro*, facilitating HTT loading into autophagolysosomes for
507 degradation.

508 Author Contributions

509 YA and DDOM conceived of experiments. FA completed preliminary work (not included). YA completed
510 the experiments in Figures 2-6. FA helped complete the SQSTM1 palmitoylation experiment in Figure 2.
511 MR helped complete the qPCR experiments in Figure 6. AD helped complete the docking experiments in
512 Figure 6. FR helped with animal studies including preparation of primary neuronal cultures. YA prepared
513 the first draft. YA prepared Figures 1-7. YA and DDOM edited the final draft.

514 Funding

515 DDOM is supported by a Natural Sciences and Engineering Research Council Discovery Grant (RGPIN-
516 2019-04617) and Huntington Society of Canada (HSC) Navigator Research Award. YA is supported by a
517 Canadian Institutes of Health Research (CIHR) Canada Graduate Scholarship Master's Award. AD is
518 supported by an HSC Undergraduate Summer Fellowship. FR is supported by a CIHR Postdoctoral
519 Fellowship Award.

520 Conflicts of Interest

521 The authors declare no conflicts of interest.

522 Acknowledgements

523 We would like to acknowledge that the University of Waterloo resides on the traditional territory of five
524 Indigenous communities, including the Ho-de-no-sau-nee-ga (Haudenosaunee), Mississaugas of the
525 Credit First Nation, Anishinabewaki, Attiwonderonk (Neutral), and Mississauga peoples, which is

526 situated on the Haldimand Tract, a land granted to the Six Nations, encompassing six miles on either

527 side of the Grand River. This land is home to many past, present, and future Indigenous peoples.

528 ## References

529 1. Fujikake, N., Shin, M. & Shimizu, S. Association Between Autophagy and Neurodegenerative
530 Diseases. *Front Neurosci* **12**, 255 (2018).
531 2. Martin, D. D. O., Ladha, S., Ehrnhoefer, D. E. & Hayden, M. R. Autophagy in Huntington disease and
532 huntingtin in autophagy. *Trends in Neurosciences* **38**, 26–35 (2015).
533 3. Suk, T. R. & Rousseaux, M. W. C. The role of TDP-43 mislocalization in amyotrophic lateral sclerosis.
534 *Mol Neurodegener* **15**, 45 (2020).
535 4. Ramzan, F., Abrar, F., Mishra, G. G., Liao, L. M. Q. & Martin, D. D. O. Lost in traffic: consequences of
536 altered palmitoylation in neurodegeneration. *Front Physiol* **14**, 1166125 (2023).
537 5. Wlodarczyk, J. *et al.* Altered Protein Palmitoylation as Disease Mechanism in Neurodegenerative
538 Disorders. *J Neurosci* **44**, e1225242024 (2024).
539 6. Parzych, K. R. & Klionsky, D. J. An Overview of Autophagy: Morphology, Mechanism, and Regulation.
540 *Antioxid Redox Signal* **20**, 460–473 (2014).
541 7. Huang, X., Zhang, J., Yao, J., Mi, N. & Yang, A. Phase separation of p62: roles and regulations in
542 autophagy. *Trends in Cell Biology* **35**, 854–865 (2025).
543 8. Pircs, K. *et al.* Distinct subcellular autophagy impairments in induced neurons from patients with
544 Huntington's disease. *Brain* **145**, 3035–3057 (2022).
545 9. Martinez-Vicente, M. *et al.* Cargo recognition failure is responsible for inefficient autophagy in
546 Huntington's disease. *Nat Neurosci* **13**, 567–576 (2010).
547 10. Walter, C. *et al.* Activation of AMPK-induced autophagy ameliorates Huntington disease pathology
548 in vitro. *Neuropharmacology* **108**, 24–38 (2016).
549 11. Ghosh, R. & Tabrizi, S. J. Clinical Features of Huntington's Disease. in *Polyglutamine Disorders* (eds
550 Nóbrega, C. & Pereira de Almeida, L.) 1–28 (Springer International Publishing, Cham, 2018).
551 doi:10.1007/978-3-319-71779-1_1.
552 12. The Huntington's Disease Collaborative Research Group. A novel gene containing a trinucleotide
553 repeat that is expanded and unstable on Huntington's disease chromosomes. *Cell* **72**, 971–983
554 (1993).
555 13. Kay, C. *et al.* Huntington disease reduced penetrance alleles occur at high frequency in the general
556 population. *Neurology* **87**, 282–288 (2016).
557 14. Saudou, F. & Humbert, S. The Biology of Huntingtin. *Neuron* **89**, 910–926 (2016).

558 15. Ochaba, J. *et al.* Potential function for the Huntingtin protein as a scaffold for selective autophagy.
559 *Proc Natl Acad Sci U S A* **111**, 16889–16894 (2014).
560 16. Rui, Y.-N. *et al.* Huntingtin Functions as a Scaffold for Selective Macroautophagy. *Nat Cell Biol* **17**,
561 262–275 (2015).
562 17. Ehrnhoefer, D. E. *et al.* Preventing mutant huntingtin proteolysis and intermittent fasting promote
563 autophagy in models of Huntington disease. *Acta Neuropathol Commun* **6**, 16 (2018).
564 18. Abrar, F. *et al.* Reduced Palmitoylation of SQSTM1/p62 in Huntington Disease Is Associated With
565 Impaired Autophagy. *FASEB J* **39**, e70549 (2025).
566 19. Alshehabi, Y., Abrar, F. & Martin, D. D. O. Sequestering sequestosome 1 via S-acylation in
567 autophagy, Huntington disease, and beyond. *Autophagy Rep* **4**, 2547975 (2025).
568 20. Chamberlain, L. H. & Shipston, M. J. The physiology of protein S-acylation. *Physiol Rev* **95**, 341–376
569 (2015).
570 21. Anwar, M. U. & van der Goot, F. G. Refining S-acylation: Structure, regulation, dynamics, and
571 therapeutic implications. *Journal of Cell Biology* **222**, e202307103 (2023).
572 22. Yanai, A. *et al.* Palmitoylation of huntingtin by HIP14is essential for its trafficking and function. *Nat*
573 *Neurosci* **9**, 824–831 (2006).
574 23. Lemarié, F. L. *et al.* Rescue of aberrant huntingtin palmitoylation ameliorates mutant huntingtin-
575 induced toxicity. *Neurobiology of Disease* **158**, 105479 (2021).
576 24. Lemarié, F. L., Sanders, S. S., Nguyen, Y., Martin, D. D. O. & Hayden, M. R. Full-length huntingtin is
577 palmitoylated at multiple sites and post-translationally myristoylated following caspase-cleavage.
578 *Front Physiol* **14**, 1086112 (2023).
579 25. Martin, D. D. O. & Sanders, S. S. Let's get fat: emergence of S-acylation as a therapeutic target in
580 Huntington disease. *Biochemical Society Transactions* **52**, 1385–1392 (2024).
581 26. Virlogeux, A. *et al.* Increasing brain palmitoylation rescues behavior and neuropathology in
582 Huntington disease mice. *Sci Adv* **7**, eabb0799 (2021).
583 27. Huang, X. *et al.* S-acylation of p62 promotes p62 droplet recruitment into autophagosomes in
584 mammalian autophagy. *Mol Cell* **83**, 3485-3501.e11 (2023).
585 28. Martin, D. D. O. *et al.* Identification of Novel Inhibitors of DLK Palmitoylation and Signaling by High
586 Content Screening. *Sci Rep* **9**, 3632 (2019).
587 29. Athira, K. V., Sadanandan, P. & Chakravarty, S. Repurposing Vorinostat for the Treatment of
588 Disorders Affecting Brain. *Neuromol Med* **23**, 449–465 (2021).

589 30. Verrillo, L., Di Palma, R., de Bellis, A., Drongitis, D. & Miano, M. G. Suberoylanilide Hydroxamic Acid
590 (SAHA) Is a Driver Molecule of Neuroplasticity: Implication for Neurological Diseases. *Biomolecules*
591 **13**, 1301 (2023).
592 31. Liao, L. M. Q., Gray, R. A. V. & Martin, D. D. O. Optimized Incorporation of Alkynyl Fatty Acid Analogs
593 for the Detection of Fatty Acylated Proteins using Click Chemistry. *J Vis Exp*
594 https://doi.org/10.3791/62107 (2021) doi:10.3791/62107.
595 32. Hayashi, T., Thomas, G. M. & Huganir, R. L. Dual Palmitoylation of NR2 Subunits Regulates NMDA
596 Receptor Trafficking. *Neuron* **64**, 213–226 (2009).
597 33. Trott, O. & Olson, A. J. AutoDock Vina: improving the speed and accuracy of docking with a new
598 scoring function, efficient optimization and multithreading. *J Comput Chem* **31**, 455–461 (2010).
599 34. McClafferty, H. & Shipston, M. J. siRNA Knockdown of Mammalian zDHHCs and Validation of mRNA
600 Expression by RT-qPCR. in *Protein Lipidation* (ed. Linder, M. E.) vol. 2009 151–168 (Springer New
601 York, New York, NY, 2019).
602 35. Hockly, E. *et al.* Suberoylanilide hydroxamic acid, a histone deacetylase inhibitor, ameliorates motor
603 deficits in a mouse model of Huntington's disease. *Proc Natl Acad Sci U S A* **100**, 2041–2046 (2003).
604 36. Davda, D. *et al.* Profiling targets of the irreversible palmitoylation inhibitor 2-bromopalmitate. *ACS*
605 *Chem Biol* **8**, 1912–1917 (2013).
606 37. Blanc, M. *et al.* SwissPalm: Protein Palmitoylation database. Preprint at
607 https://doi.org/10.12688/f1000research.6464.1 (2015).
608 38. Ji, G. *et al.* Global Analysis of Endogenously Intact S-Acylated Peptides Reveals Localization
609 Differentiation of Heterogeneous Lipid Chains in Mammalian Cells. *Anal Chem* **95**, 13055–13063
610 (2023).
611 39. Hill, S. M. *et al.* VCP/p97 regulates Beclin-1-dependent autophagy initiation. *Nat Chem Biol* **17**, 448–
612 455 (2021).
613 40. Ramzan, F. *et al.* Fatty links between multisystem proteinopathy and small VCP-interacting protein.
614 *Cell Death Discov* **10**, 358 (2024).
615 41. Vanderhaeghe, S. *et al.* A pathogenic mutation in the ALS/FTD gene VCP induces mitochondrial
616 hypermetabolism by modulating the permeability transition pore. *Acta Neuropathologica*
617 *Communications* **12**, 161 (2024).
618 42. Klionsky, D. J. *et al.* Guidelines for the use and interpretation of assays for monitoring autophagy
619 (4th edition)1. *Autophagy* **17**, 1–382 (2021).

620 43. Alshehabi, Y. Restoring p62 Palmitoylation as a Viable Therapeutic Approach for Mitigating the
621 Effects of Huntington Disease. *UWSpace* (2025).
622 44. Abrami, L. *et al.* Identification and dynamics of the human ZDHHC16-ZDHHC6 palmitoylation
623 cascade. *eLife* **6**, e27826 (2017).
624 45. Plain, F. *et al.* Control of protein palmitoylation by regulating substrate recruitment to a zDHHC-
625 protein acyltransferase. *Commun Biol* **3**, 411 (2020).
626 46. Zheng, W. *et al.* S-palmitoylation modulates ATG2-dependent non-vesicular lipid transport during
627 starvation-induced autophagy. *EMBO J* **44**, 2596–2619 (2025).
628 47. Kim, S. W. *et al.* Palmitoylation controls trafficking of the intracellular Ca2+ channel
629 MCOLN3/TRPML3 to regulate autophagy. *Autophagy* **15**, 327–340 (2018).
630 48. Mielcarek, M. *et al.* SAHA decreases HDAC 2 and 4 levels in vivo and improves molecular
631 phenotypes in the R6/2 mouse model of Huntington's disease. *PLoS One* **6**, e27746 (2011).
632 49. Zuccato, C. & Cattaneo, E. Role of brain-derived neurotrophic factor in Huntington's disease. *Prog*
633 *Neurobiol* **81**, 294–330 (2007).
634 50. Benn, C. L., Fox, H. & Bates, G. P. Optimisation of region-specific reference gene selection and
635 relative gene expression analysis methods for pre-clinical trials of Huntington's disease. *Mol*
636 *Neurodegener* **3**, 17 (2008).
637 51. Gharami, K., Xie, Y., An, J. J., Tonegawa, S. & Xu, B. Brain-derived neurotrophic factor over-
638 expression in the forebrain ameliorates Huntington's disease phenotypes in mice. *J Neurochem* **105**,
639 369–379 (2008).
640 52. Mielcarek, M. *et al.* HDAC4 reduction: a novel therapeutic strategy to target cytoplasmic huntingtin
641 and ameliorate neurodegeneration. *PLoS Biol* **11**, e1001717 (2013).
642 53. Federspiel, J. D., Greco, T. M., Lum, K. K. & Cristea, I. M. Hdac4 Interactions in Huntington's Disease
643 Viewed Through the Prism of Multiomics. *Mol Cell Proteomics* **18**, S92–S113 (2019).
644 54. Mori-Konya, C. *et al.* p97/valosin-containing protein (VCP) is highly modulated by phosphorylation
645 and acetylation. *Genes Cells* **14**, 483–497 (2009).
646 55. Guo, X. *et al.* VCP recruitment to mitochondria causes mitophagy impairment and
647 neurodegeneration in models of Huntington's disease. *Nat Commun* **7**, 12646 (2016).
648